INTERNATIONAL JOURNAL FOR NUMERICAL METHODS IN FLUIDS, VOL. 21, 617–640 (1995)

OPERATOR-SPLITTING METHODS FOR THE INCOMPRESSIBLE NAVIER–STOKES EQUATIONS ON NON-STAGGERED GRIDS. PART 1: FIRST-ORDER SCHEMES

ALEXANDER G. CHURBANOV, ANDREI N. PAVLOV AND PETER N. VABISHCHEVICH

Institute for Mathematical Modelling, Russian Academy of Sciences, 4 Miusskaya Sq., Moscow 125047, Russia

SUMMARY

New implicit finite difference schemes for solving the time-dependent incompressible Navier–Stokes equations using primitive variables and non-staggered grids are presented in this paper. *A priori* estimates for the discrete solution of the methods are obtained. Employing the operator approach, some requirements on the difference operators of the scheme are formulated in order to derive a scheme which is essentially consistent with the initial differential equations. The operators of the scheme inherit the fundamental properties of the corresponding differential operators and this allows *a priori* estimates for the discrete solution to be obtained. The estimate is similar to the corresponding one for the solution of the differential problem and guarantees boundedness of the solution. To derive the consistent scheme, special approximations for convective terms and div and grad operators are employed. Two variants of time discretization by the operator-splitting technique are considered and compared. It is shown that the derived scheme has a very weak restriction on the time step size. A lid-driven cavity flow has been predicted to examine the stability and accuracy of the schemes for Reynolds number up to 3200 on the sequence of grids with 21×21, 41×41, 81×81 and 161×161 grid points.

KEY WORDS: incompressible viscous flow; numerical methods; non-staggered grids; consistent approximations of operators; operator-splitting technique

1. INTRODUCTION

The most commonly used approach to study incompressible and slightly compressible viscous flows is based on SIMPLE-like procedures (see e.g. Reference 1) and the MAC-type staggered grid.[2] For this grid all scalar variables including the pressure are located at the centre of a control volume, whereas velocity components are referred to its corresponding faces. Using such a grid, it is easy to construct a difference scheme for the continuity and momentum equations and then to derive the discrete Poisson equation for the pressure (or pressure correction) with the standard compact difference Laplace operator by means of algebraic transformations of the initial grid equations.

However, the use of non-staggered grids seems to be very attractive. It is apparent that on going from a staggered grid to a collocated one, we can essentially simplify the numerical algorithms and reduce their computation cost. Further, methods based on the non-staggered grid are more uniform and thus allow the easy use of local grid adaptation, non-orthogonal co-ordinates and multigrid techniques in order to increase the solution accuracy. Finally, the numerical implementation of boundary conditions becomes more accurate and natural in this case.

CCC 0271–2091/95/080617–24

Received May 1994
Revised February 1995

Simple usage of the collocated grid and second-order central difference approximations for the divergence and gradient operators leads to so-called 'checker-board' effects[1] in the pressure and velocity fields if the velocity–pressure decoupling is performed via the Poisson equation for the pressure. Instead of the standard Laplace operator (five-point in the 2D case) one obtains it on an extended stencil with splitting of grid points into some non-intersecting sets. Pressure and velocity oscillations occur in this situation.[1]

Many different methods have been proposed by various authors (see e.g. References 3–13) to avoid these checker-board effects on the non-staggered grid. However, all these techniques employ (in an explicit or implicit way) non-standard approximations of the continuity equation. As a rule, non-standard interpolation of the velocity values at control volume faces is utilized to form the discrete continuity equation. Thus the discrete continuity equation perturbed by inserting additional terms with pressure values is actually used in calculations. This technique sometimes leads to physically incorrect velocity values at control volume faces.

New difference schemes for viscous incompressible flow predictions on non-staggered grids are developed and investigated in the present work. The main feature of the schemes is their consistency with the initial differential equations in terms of the fundamental properties of the corresponding operators.[14,15] The operator approach is used to study approximations for the Navier–Stokes equations and some requirements on the difference operators are formulated. The required properties of the operators allow *a priori* estimates for the discrete solution to be obtained. The estimate is similar to the corresponding one for a solution of the differential problem and guarantees boundedness of the solution.

To derive difference operators with the desired properties, a special second-order approximation for convective terms is used. Several variants of consistent approximations for the div and grad operators are considered. In this part of the investigation the particular emphasis is on the first-order opposite differencing (forward and backward differences) for these operators that leads to the Poisson equation with the standard compact stencil on the non-staggered grid. A study of second-order approximations will be presented in the next part of the work.

The operator-splitting technique[16–18] is employed to obtain a time discretization which allows efficient implementation. This approach is in common use in non-linear mechanics and CFD (see e.g. References 19–23) for velocity–pressure decoupling, implementation of non-linearity, treatment of additional source terms in the Navier–Stokes equations, etc. Two variants of the operator-splitting technique (Peaceman–Rachford[24] and Douglas–Rachford[25] types) are considered in detail and compared in this work. The stability and accuracy of the schemes are demonstrated with the solution of a lid-driven cavity flow problem.

2. DIFFERENTIAL PROBLEM

The unsteady Navier–Stokes equations for an incompressible fluid flow in a 2D closed domain Ω with a piecewise smooth boundary $\partial\Omega$ can be written in the dimensionless form

$$\frac{\partial \mathbf{v}}{\partial t} + \mathscr{V}(\mathbf{v})\mathbf{v} + \operatorname{grad} p - \frac{1}{Re}\operatorname{div}\operatorname{grad}\mathbf{v} = \mathbf{f}(\mathbf{x}, t), \quad \mathbf{x} \in \Omega, \quad 0 < t \leqslant \Theta, \tag{1}$$

$$\operatorname{div}\mathbf{v} = 0, \quad \mathbf{x} \in \Omega, \quad 0 < t \leqslant \Theta, \tag{2}$$

with no-slip, no-permeability boundary conditions on the fixed rigid boundary $\partial\Omega$,

$$\mathbf{v}(\mathbf{x}, t) = 0, \quad \mathbf{x} \in \partial\Omega, \quad 0 < t \leqslant \Theta, \tag{3}$$

and the divergence-free initial conditions

$$\mathbf{v}(\mathbf{x},\ 0) = \mathbf{v}_0(\mathbf{x}), \quad \mathbf{x} \in \Omega. \tag{4}$$

Here $\mathbf{v} = (v_1, v_2)$ is the velocity vector, t is the time, $\mathbf{x} = (x_1, x_2)$ represents the Cartesian coordinates, p is the pressure, Re is the Reynolds number and $\mathbf{f}$ is the volumetric force vector. It should be noted that the initial and boundary conditions must be prescribed consistently. The only singularity allowed is with the boundary conditions for the tangential velocity, whereas in respect of all other initial data and boundary conditions this initial boundary value problem has to be well posed.[26] The two-dimensional equations are considered here only for simplicity. There is no problem in extending the results presented below to the 3D case.

In equation (1) the operator $\mathscr{V}(\mathbf{v})$ represents the convective terms and can be written in various forms. The advective (non-divergence) form is

$$\mathscr{V}(\mathbf{v})\mathbf{v} = (\mathbf{v} \cdot \operatorname{grad})\mathbf{v}.$$

Here and below we use the terminology of Gresho.[26] Using the incompressibility constraint (2), we can rewrite $\mathscr{V}(\mathbf{v})$ in the divergence form

$$\mathscr{V}(\mathbf{v})\mathbf{v} = \operatorname{div}(\mathbf{vv})$$

or in the skew-symmetric form

$$\mathscr{V}(\mathbf{v})\mathbf{v} = \tfrac{1}{2}[(\mathbf{v} \cdot \operatorname{grad})\mathbf{v} + \operatorname{div}(\mathbf{vv})], \tag{5}$$

which is simply the half-sum of the two previous forms. It should be noted that all these forms are equivalent in the continuum case but generally not equivalent in the discrete case.

An additional relation can be introduced for pressure uniqueness:

$$\int_\Omega p(\mathbf{x},\ t)\mathrm{d}\mathbf{x} = 0, \quad 0 < t \leqslant \Theta. \tag{6}$$

Thus we have now the complete system of equations (1)–(4) and (6) for the determination of a fluid flow in the domain Ω at any time instant $t > 0$.

3. *A PRIORI* ESTIMATE FOR THE SOLUTION OF THE DIFFERENTIAL PROBLEM

Let us introduce the Hilbert space $\mathscr{H} = L_2(\Omega)$ of functions with the scalar product

$$(u,\ w)_1 = \int_\Omega u(\mathbf{x})w(\mathbf{x})\mathrm{d}\mathbf{x}, \quad u(\mathbf{x}),\ w(\mathbf{x}) \in \mathscr{H},$$

and the corresponding norm $\| u \| = \sqrt{((u, u)_1)}$. For vectors $\mathbf{u}$ we can define the Hilbert space $\mathscr{H}^2$ as the direct sum $\mathscr{H}^2 = \mathscr{H} \oplus \mathscr{H}$ with the scalar product

$$(\mathbf{u},\ \mathbf{w})_2 = \sum_{\alpha=1}^{2}(u_\alpha,\ w_\alpha)_1$$

and the norm $\| \mathbf{u} \| = \sqrt{((\mathbf{u}, \mathbf{u})_2)}$.

Let $\mathscr{H}^2_*$ be the subspace of $\mathscr{H}^2$ containing solenoidal functions, i.e. functions for which the incompressibility constraint (2) holds. We can rewrite equations (1) and (2) in this subspace as a single equation in the operator form

$$\frac{\mathrm{d}\mathbf{v}}{\mathrm{d}t} + \mathscr{V}(\mathbf{v})\mathbf{v} + \mathscr{P}\mathbf{v} + \mathscr{N}\mathbf{v} = \mathbf{f}, \quad 0 < t \leqslant \Theta, \quad \mathbf{v} \in \mathscr{H}^2_*, \tag{7}$$

where $\mathbf{f}(\mathbf{x}, t)$ belongs to $\mathscr{H}^2$. Here we use the notation $\mathrm{d}/\mathrm{d}t$ instead of $\partial/\partial t$, since equation (7) is not formally a partial differential equation. We use the following notation for the operators: $\mathscr{V}(\mathbf{v})$, the convective transport operator in the skew-symmetric form (5); $\mathscr{P}$, the gradient operator $\mathscr{P}\mathbf{v} = \mathrm{grad}p$—we can formally consider the operator $\mathscr{P}$ as one operating on the velocity $\mathbf{v} \in \mathscr{H}^2_*$; $\mathscr{N}$, the diffusive transport operator $-Re^{-1}$ div grad.

The incompressibility constraint is already incorporated in this operator equation. We emphasize that this equation has been introduced only in order to reduce the number of formulae. Next we use for the pressure gradient the notation $\mathscr{P}\mathbf{v}$, i.e. formally it is written as an operator on the divergence-free velocity. In such a reduced formulation of equations the fundamental property of differential operators that the gradient and divergence operators are conjugate to each other[14,15] (with minus sign) can be treated as the skew-symmetric property of the operator $\mathscr{P}$.

It is well known (see e.g. References 14 and 15) that these operators in the subspace $\mathscr{H}^2_*$ of functions with zero values on the boundary $\partial\Omega$ have the basic properties

$$\mathscr{V}(\mathbf{v}) = -\mathscr{V}^*(\mathbf{v}) \quad \text{(skew-symmetric)}, \tag{8}$$

$$\mathscr{P} = -\mathscr{P}^* \quad \text{(skew-symmetric)}, \tag{9}$$

$$\mathscr{N} = \mathscr{N}^* > 0 \quad \text{(symmetric and positive)}. \tag{10}$$

It should be emphasized that properties (8)–(10) are valid only for the vectors from $\mathscr{H}^2_*$ which are solenoidal and have uniform zero values on the boundary. Next, if the form (5) of the operator $\mathscr{V}(\mathbf{v})$ is used, $\mathscr{V}(\mathbf{v})$ will be skew-symmetric for any vector $\mathbf{v}$ with zero values on the boundary, not only for the solenoidal vectors. To verify the skew-symmetric property of the operator $\mathscr{P}$, one can write

$$(\mathscr{P}\mathbf{v},\ \mathbf{v})_2 = (\mathrm{grad}p,\ \mathbf{v})_2 = -(p,\ \mathrm{div}\mathbf{v})_1 = 0.$$

Here we use the following well-known fact: an operator $\mathscr{A}$ is skew-symmetric if and only if $(\mathscr{A}\varphi,\ \varphi) = 0$ for any φ from the considered space. Property (10) holds owing to the fact that the diffusive transport operator is the Laplace operator with constant coefficient $-1/Re$.

To get the simplest *a priori* estimate for the solution of problem (7) with the initial conditions (4), let us multiply equation (7) by $\mathbf{v}$ and take the scalar product in $\mathscr{H}^2_*$:

$$\|\mathbf{v}\| \frac{\mathrm{d}\|\mathbf{v}\|}{\mathrm{d}t} + (\mathscr{V}(\mathbf{v})\mathbf{v},\ \mathbf{v})_2 + (\mathscr{P}\mathbf{v},\ \mathbf{v})_2 + (\mathscr{N}\mathbf{v},\ \mathbf{v})_2 = (\mathbf{f},\ \mathbf{v})_2. \tag{11}$$

Using the above-mentioned basic properties (8)–(10) of the operators $\mathscr{V}(\mathbf{v})$, $\mathscr{P}$ and $\mathscr{N}$ and the Schwarz inequality, we obtain

$$\frac{\mathrm{d}\|\mathbf{v}\|}{\mathrm{d}t} \leqslant \|\mathbf{f}\|.$$

Thus, using the initial conditions (4), the following estimate can be derived:

$$\|\mathbf{v}(\mathbf{x},\ t)\| \leqslant \|\mathbf{v}_0(\mathbf{x})\| + \int_0^t \|f(\mathbf{x},\ s)\|\mathrm{d}s. \tag{12}$$

Estimate (12) provides boundedness of the problem solution. It also provides unconditional stability of the trivial (zero) solution in respect of the right-hand side and initial data for this non-linear problem.

4. DISCRETE PROBLEM

Let us construct finite difference operators satisfying properties (8)–(10) of the parent operators. To simplify the presentation, we shall use a grid with uniform spacings h_1 and h_2 in the rectangular domain $\Omega = \{(x_1, x_2) \mid 0 < x_\alpha < l_\alpha,\ \alpha = 1, 2\}$.

Let ω be the internal point set

$$\omega = \{(x_{1i}, x_{2j}) \mid x_{1i} = (i-1)h_1,\ x_{2j} = (j-1)h_2,\ h_1 = l_1/(N_1-1),\ h_2 = l_2/(N_2-1),$$
$$i = 2, \ldots, N_1 - 1,\ j = 2, \ldots, N_2 - 1\},$$

$\partial\omega$ be the set of boundary points (without corner points) and $\bar{\omega}$ be the set of internal and boundary points, $\bar{\omega} = \omega \cup \partial\omega$ (see Figure 1).

As in the differential case we can again introduce the finite-dimensional Hilbert space H with the scalar product (we use the same notation for the discrete case)

$$(y,\ z)_1 = \sum_{\mathbf{x}\in\omega} y(\mathbf{x})z(\mathbf{x})h_1h_2$$

and the Hilbert space H^2 as the direct sum $H^2 = H \oplus H$ with the corresponding scalar product

$$(\mathbf{y},\ \mathbf{z})_2 = \sum_{\alpha=1}^{2}(y_\alpha,\ z_\alpha)_1$$

and the norm

$$\|\mathbf{y}\| = \sqrt{((\mathbf{y},\ \mathbf{y})_2)}.$$

We shall use the standard notation for the first- and second-order spatial approximations.[17,18] For example, the foward, backward and central differences with respect to the co-ordinate x_1 are

$$(y_{x_1})_{i,j} = \frac{y_{i+1,j} - y_{i,j}}{h_1}, \qquad (y_{\bar{x}_1})_{i,j} = \frac{y_{i,j} - y_{i-1,j}}{h_1}, \qquad (y_{\mathring{x}_1})_{i,j} = \frac{y_{i+1,j} - y_{i-1,j}}{2h_1}.$$

We shall denote by Λ the discrete Laplace operator with the standard compact five-point stencil:

$$\Lambda y = -\sum_{\alpha=1}^{2} y_{\bar{x}_\alpha x_\alpha}. \tag{13}$$

In the subspace H of grid functions with zero values on the grid boundary $\partial\omega$ the Laplace operator Λ is symmetric and positive definite, $\Lambda = \Lambda^* > 0$ (see e.g. References 17 and 18).

Let us consider also the space H^2_* as the subspace of H^2 containing only solenoidal vector functions. The solenoidal functions satisfy some discrete analogue of the incompressibility constraint,

$$\mathrm{div}_h \mathbf{w} = 0, \quad \mathbf{x} \in \omega^*, \tag{14}$$

where ω^* is a subset of $\bar{\omega}$ (specified below).

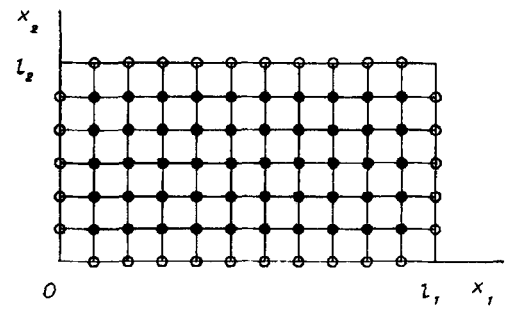

Figure 1. Grid arrangement showing the internal point set ω (●) and the set of boundary points $\partial\omega$ (○)

Let us consider the semidiscrete (continuous in time and discrete in space) problem

$$\frac{d\mathbf{w}}{dt} + V(\mathbf{w})\mathbf{w} + P\mathbf{w} + N\mathbf{w} = \mathbf{f}, \quad \mathbf{w} \in H_*^2, \quad 0 < t \leqslant \Theta, \tag{15}$$

$$\mathbf{w}(\mathbf{x}, 0) = \mathbf{v}_0(\mathbf{x}), \quad \mathbf{x} \in \omega. \tag{16}$$

We introduce such a reduced formulation of equations in exactly the same manner as has been done above for the differential problem (7). It should be noted that the original Dirichlet boundary conditions for the velocity (and only for the velocity) are already incorporated in this semidiscrete problem.

In accordance with the skew-symmetric form (5), let us consider the next second-order approximation of the convective terms,

$$V(\mathbf{w})\mathbf{y} = \sum_{\alpha=1}^{2} \tfrac{1}{2}\left((\omega_\alpha \mathbf{y})_{\mathring{x}_\alpha} + \omega_\alpha \mathbf{y}_{\mathring{x}_\alpha}\right). \tag{17}$$

It is easy to show that

$$(V(\mathbf{w})\mathbf{y}, \mathbf{y}) = 0 \tag{18}$$

for any $\mathbf{w}, \mathbf{y} \in H^2$ with zero values on $\partial\omega$, i.e. this discrete operator inherits the skew-symmetric property of the parent differential operator $\mathscr{V}(\mathbf{v})$.

Let us consider the next discrete operator

$$N = \frac{1}{Re}\Lambda, \tag{19}$$

where Λ is taken as (13). This operator inherits property (10) of the corresponding operator $\mathscr{N}$, i.e. $N = N^* > 0$, owing to the fact that $\Lambda = \Lambda^* > 0$.

Now we shall construct the skew-symmetric discrete operator P. The difference operator P is defined by the expression

$$P\mathbf{w} = \operatorname{grad}_h p, \quad \mathbf{w} \in H_*^2. \tag{20}$$

The operator P will be skew-symmetric if the following equation is valid:

$$(P\mathbf{w}, \mathbf{w})_2 = 0, \quad \mathbf{w} \in H_*^2. \tag{21}$$

In order to obtain the skew-symmetric operator P for which (21) is valid, one has to consider consistent approximations for the grad and div operators. The consistency of the operators grad_h and div_h lies in the fulfilment of the equality

$$(\operatorname{grad}_h p, \mathbf{w})_2 = -(p, \operatorname{div}_h \mathbf{w})_1^*, \tag{22}$$

where

$$(v, y)_1^* = \sum_{\mathbf{x} \in \omega^*} v(\mathbf{x}) y(\mathbf{x}) h_1 h_2. \tag{23}$$

It is evident that equality (21) for the operator P defined by (20) will be valid if the operators grad_h and div_h are constructed so that (22) is fulfilled and $\operatorname{div}_h \mathbf{w} = 0$ at $\mathbf{x} \in \omega^*$. Thus P will be skew-symmetric in this case.

In order to obtain mutually consistent operators grad_h and div_h, we shall define the operator grad_h and then utilize equation (22) to derive the concrete form of the operator div_h and the subset $\omega^* \in \bar{\omega}$.

Choosing the backward differences for the gradient operator as

$$\operatorname{grad}_h p = (p_{\bar{x}_1}, p_{\bar{x}_2}), \quad \mathbf{x} \in \omega, \tag{24}$$

we obtain from (22)

$$(\mathrm{grad}_h p,\ \mathbf{w})_2 = \sum_{\alpha=1}^{2} (p_{\bar{x}_\alpha},\ w_\alpha)_1 = -\sum_{\alpha=1}^{2} (p,\ (w_\alpha)_{x_\alpha})_1^*.$$

Thus we have the forward differences for the divergence operator in this case as

$$\mathrm{div}_h \mathbf{w} = (w_1)_{x_1} + (w_2)_{x_2}, \quad \mathbf{x} \in \omega^*. \tag{25}$$

It is clear from (22) that the pressure p and the operator div_h in the form (25) must be defined at points of the set ω^* (see Figure 2), where

$$\omega^* = \{(x_{1i}, x_{2j}) \mid x_{1i} = (i-1)h_1,\ x_{2j} = (j-1)h_2,\ i = 1,\ 2,\ \ldots,\ N_1 - 1,\ j = 1,\ 2,\ \ldots,\ N_2 - 1,\ i + j \neq 2\}.$$

Thus the couple

$$\mathrm{grad}_h p = (p_{\bar{x}_1},\ p_{\bar{x}_2}), \qquad \mathrm{div}_h \mathbf{w} = (w_1)_{x_1} + (w_2)_{x_2}, \tag{26}$$

where div_h is defined in ω^*, provides the skew-symmetric property of the operator P.

It is easy to see that in the 2D case four different combinations of the forward and backward approximations exist for these coupled operators. The other three couples are

$$\mathrm{grad}_h p = (p_{x_1},\ p_{x_2}), \qquad \mathrm{div}_h \mathbf{w} = (w_1)_{\bar{x}_1} + (w_2)_{\bar{x}_2}, \tag{27}$$

$$\mathrm{grad}_h p = (p_{\bar{x}_1},\ p_{x_2}), \qquad \mathrm{div}_h \mathbf{w} = (w_1)_{x_1} + (w_2)_{\bar{x}_2}, \tag{28}$$

$$\mathrm{grad}_h p = (p_{x_1},\ p_{\bar{x}_2}), \qquad \mathrm{div}_h \mathbf{w} = (w_1)_{\bar{x}_1} + (w_2)_{x_2}, \tag{29}$$

From the theoretical standpoint all these combinations (26)–(29) are equivalent. However, the accuracy of the computed results may be different for the various cases when a particular flow is predicted.

It should be noted that in spite of the first-order truncation error the idea of employing opposite differences for these terms is quite popular in CFD. A good example is the paper by Reggio and Camarero,[3] who used forward and backward differences for mass and pressure gradients respectively on the basis of an upwinding strategy. Other applications are given in references cited in that work.

The use of the standard central difference approximation for grad_h leads to the same approximation for div_h and yields for the pressure evaluation the discrete Laplace operator

$$-\mathrm{div}_h \mathrm{grad}_h y = -\sum_{\alpha=1}^{2} y_{\mathring{x}_\alpha \mathring{x}_\alpha}$$

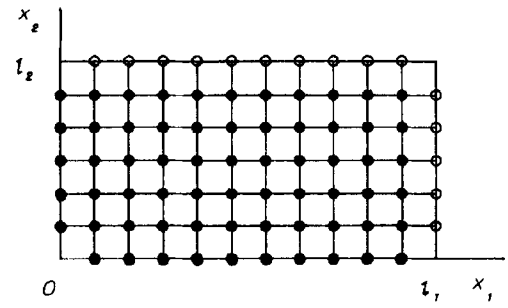

Figure 2. The set ω^* (●)

with the extended stencil and the above-mentioned checker-board effects. Only first-order differences will be considered in detail in the present paper. The use of central differences in the framework of the developed approach will be discussed in the next part of the study.

Thus the considered difference operators $V(\mathbf{w})$, P and N defined by (17), (26) and (19) respectively inherit the main properties of the corresponding differential operators, namely

$$V(\mathbf{v}) = -V^*(\mathbf{v}) \quad \text{(skew-symmetric)}, \tag{30}$$

$$P = -P^* \quad \text{(skew-symmetric)}, \tag{31}$$

$$N = N^* > 0 \quad \text{(symmetric and positive definite)}. \tag{32}$$

One can easily obtain an *a priori* estimate

$$\|\mathbf{w}(\mathbf{x}, t)\| \leq \|\mathbf{v}_0(\mathbf{x})\| + \int_0^t \|f(\mathbf{x}, s)\| \mathrm{d}s$$

for the semidiscrete problem (15), (16) by repeating calculation (11).

5. TIME DISCRETIZATION BY OPERATOR SPLITTING

Now time discretization of the space-discrete problem (15), (16) and its numerical implementation will be considered. It is well known that the operator-splitting technique[16–18] is a very popular approach to constructing efficient numerical methods for unsteady problems. This approach is in common use in CFD as well (see e.g. References 19–21). Among recent contributions the papers by Maday *et al.*[22] and Natarajan[23] should be mentioned. In the present study this general methodology will be used to solve the problem of velocity–pressure decoupling.

We shall split the operators of the momentum equation into two parts associated with velocity and pressure respectively and rewrite the semidiscrete operator equation (15) as

$$\frac{\mathrm{d}\mathbf{w}}{\mathrm{d}t} + (A_1 + A_2)\mathbf{w} = \mathbf{f}, \quad 0 < t \leqslant \Theta, \tag{33}$$

where

$$A_1 = V(\mathbf{w}) + N, \qquad A_2 = P. \tag{34}$$

The operator $V(\mathbf{w})$ is non-linear. The fundamental property (30) has been proved for this operator for any $\mathbf{w}$. Thus we can linearize this operator using the value $\mathbf{w}^n$ from the previous time level, i.e. everywhere below $A_1 = V(\mathbf{w}^n) + N$. Here superscripts n and $n+1$ are used to denote successive time levels of the time grid $t^n = n\tau$, $n = 1, 2, \ldots, N_\tau$ $\tau = \Theta$.

It is well known from the operator theory of difference schemes[18] that additive schemes (including ADI) with two operators A_1 and A_2 are unconditionally stable for linear problems with $A_1 \geqslant 0$ and $A_2 \geqslant 0$. In the considered case, in view of the basic properties (30)–(32), we have $A_1 > 0$ and $A_2 = -A_2^*$ (the proof of the fact that $N > 0$ and hence $A_1 > 0$ can be found in Reference 27, Vol. 2, p. 31 along with other results of the operator theory of difference schemes). Thus we can use several variants of the operator-splitting technique to construct unconditionally stable (in a linear sense) schemes.

Let us consider the known factorized scheme[17,18] for equation (33),

$$(E + \tau\sigma A_1)(E + \tau\sigma A_2)\frac{\mathbf{w}^{n+1} - \mathbf{w}^n}{\tau} + (A_1 + A_2)\mathbf{w}^n = \mathbf{f}^n, \quad \sigma \geqslant 0. \tag{35}$$

By introducing an intermediate velocity field, we can pass on from the factorized scheme (35) to the additive scheme. If the superscript $n+\frac{1}{2}$ denotes intermediate values, then, defining

$$\mathbf{w}^{n+1/2} = \sigma\mathbf{w}^{n+1} + (1-\sigma)\mathbf{w}^n + \sigma^2\tau A_2(\mathbf{w}^{n+1} - \mathbf{w}^n),$$

we can rewrite equation (35) as

$$\frac{\mathbf{w}^{n+1/2} - \mathbf{w}^n}{\tau\sigma} + A_1\mathbf{w}^{n+1/2} + A_2\mathbf{w}^n = \mathbf{f}^n, \tag{36}$$

$$\frac{\mathbf{w}^{n+1} - \mathbf{w}^n}{\tau} + A_1\mathbf{w}^{n+1/2} + A_2[\sigma\mathbf{w}^{n+1} + (1-\sigma)\mathbf{w}^n] = \mathbf{f}^n. \tag{37}$$

Setting $\sigma = 0{\cdot}5$, we obtain an additive scheme that is similar to the well-known Peaceman–Rachford scheme[24] for two-dimensional heat conduction problems. This method has formally second-order accuracy with respect to time. Setting $\sigma = 1$, we obtain an additive scheme for the momentum equation that is similar to the well-known Douglas–Rachford scheme.[25] It was found from calculations that this scheme is certainly preferred over the Peaceman–Rachford-type scheme, so more attention is paid below to the Douglas–Rachford-type scheme.

For the numerical implementation of the Douglas–Rachford-type scheme we obtain from (36) and (37) for $\sigma = 1$

$$\frac{\mathbf{w}^{n+1/2}}{\tau} + A_1\mathbf{w}^{n+1/2} + A_2\mathbf{w}^n = \mathbf{f}^n, \quad \mathbf{x} \in \omega, \tag{38}$$

$$\frac{\mathbf{w}^{n+1} - \mathbf{w}^n}{\tau} + A_1\mathbf{w}^{n+1/2} + A_2\mathbf{w}^{n+1} = \mathbf{f}^n, \quad \mathbf{x} \in \omega, \tag{39}$$

$$\mathrm{div}_h\mathbf{w}^{n+1} = 0, \quad \mathbf{x} \in \omega^*. \tag{40}$$

This scheme is very similar to the SIMPLEC-type pressure correction (predictor–corrector) algorithm in the time-dependent formulation. It has formally first-order accuracy with respect to time.

So far in this section we have not taken into account any particular form of the difference operators. Now we shall take this into consideration and discuss the numerical realization of the scheme (38)–(40). To implement the scheme (38)–(40), one can subtract equation (38) from (39) and obtain the so-called stabilizing correction equation

$$\frac{\mathbf{w}^{n+1} - \mathbf{w}^{n+1/2}}{\tau} + A_2(\mathbf{w}^{n+1} - \mathbf{w}^n) = 0, \quad \mathbf{x} \in \omega, \tag{41}$$

or, taking into account that $A_2 = \mathrm{grad}_h$,

$$\frac{\mathbf{w}^{n+1} - \mathbf{w}^{n+1/2}}{\tau} + \mathrm{grad}_h(p^{n+1} - p^n) = 0, \quad \mathbf{x} \in \omega. \tag{42}$$

Let us express $\mathbf{w}^{n+1}$ from (42) as

$$\mathbf{w}^{n+1} = \mathbf{w}^{n+1/2} - \tau \cdot \mathrm{grad}_h(p^{n+1} - p^n), \quad \mathbf{x} \in \omega, \tag{43}$$

and substitute it into the incompressibility constraint (40), taking into account that $\mathbf{w}^{n+1} = 0$ on the boundary $\partial\omega$.

Denoting $\delta p = p^{n+1} - p^n$, we derive the Poisson equation to evaluate the pressure correction δp as

$$\mathrm{div}_h\mathrm{grad}_h\delta p = \frac{1}{\tau}\mathrm{div}_h\mathbf{w}^{n+1/2}, \quad \mathbf{w} \in \omega, \tag{44}$$

where

$$\mathrm{div}_h \mathbf{w} = (w_1)_{x_1} + (w_2)_{x_2}, \qquad \mathrm{div}_h \mathrm{grad}_h \delta p = \delta p_{\bar{x}_1 x_1} + \delta p_{\bar{x}_2 x_2}.$$

It should be noted again that the original Dirichlet boundary conditions for the velocity (and only for the velocity) are already incorporated in this discrete problem. There is no problem with boundary conditions for the pressure correction Poisson equation in such an approach.[28,29]

More strictly, at grid points adjacent to the right and upper boundaries the difference equations with the four-point stencil are obtained and they do not include the boundary points. However, equation (44) will be valid at these points if, in order to simplify the implementation of the method, we extend the definition of the pressure correction δp to the set $\gamma = \bar{\omega} \backslash \omega^*$ by setting

$$\begin{aligned} &\delta p_{\bar{x}_1} = 0, \qquad x_1 = l_1, \qquad x_2 = (j-1)h_2, \quad j = 2,\ 3,\ \ldots,\ N_2 - 1, \\ &\delta p_{\bar{x}_2} = 0, \qquad x_2 = l_2, \qquad x_1 = (i-1)h_1, \quad i = 2,\ 3,\ \ldots,\ N_1 - 1. \end{aligned} \tag{45}$$

Equations (45) may be treated as the Neumann boundary conditions at the right and upper boundaries for the Poisson equation (44).

At the left and lower boundaries, taking into account the boundary condition $\mathbf{w}^{n+1} = 0$ at $\mathbf{x} \in \partial\omega$ and expression (43) adjacent to the boundary points, we derive from the incompressibility constraint

$$\frac{(w_1^{n+1})_{i+1,j} - (w_1^{n+1})_{i,j}}{h_1} + \frac{(w_2^{n+1})_{i,j+1} - (w_2^{n+1})_{i,j}}{h_2} = 0,$$
$$i = 2,\ 3,\ \ldots,\ N_1 - 1,\ j = 1, \quad i = 1,\ j = 2,\ 3,\ \ldots,\ N_2 - 1,$$

the equations

$$\begin{aligned} (\delta p_{\bar{x}_1})_{2,j} &= \frac{1}{\tau}(w_1)_{2,j}^{n+1/2}, \quad j = 2,\ 3,\ \ldots,\ N_2 - 1, \\ (\delta p_{\bar{x}_2})_{i,2} &= \frac{1}{\tau}(w_2)_{i,2}^{n+1/2}, \quad i = 2,\ 3,\ \ldots,\ N_1 - 1, \end{aligned} \tag{46}$$

which are treated as the Neumann boundary conditions at the left and lower boundaries for this equation. Then we have the Poisson equation (44) with the Neumann boundary conditions (45) and (46) to evaluate the pressure correction δp when the intermediate velocity $\mathbf{w}^{n+1/2}$ is known.

The final equations are now as follows:

(i) evaluation of the intermediate velocity,

$$\frac{w_\alpha^{n+1/2} - w_\alpha^n}{\tau} + \tfrac{1}{2}(w_1^n (w_\alpha^{n+1/2})_{\mathring{x}_1} + w_2^n (w_\alpha^{n+1/2})_{\mathring{x}_2} + (w_1^n w_\alpha^{n+1/2})_{\mathring{x}_1} + (w_2^n w_\alpha^{n+1/2})_{\mathring{x}_2})$$
$$- \frac{1}{Re}((w_\alpha^{n+1/2})_{x\bar{x}} + (w_\alpha^{n+1/2})_{y\bar{y}}) + p_{\bar{x}_\alpha}^n = 0, \ \mathbf{x} \in \omega, \quad \alpha = 1,\ 2, \tag{47}$$

(ii) calculation of the pressure correction,

$$\delta p_{\bar{x}_1 x_1} + \delta p_{\bar{x}_2 x_2} = \frac{1}{\tau}((w_1^{n+1/2})_{x_1} + (w_2^{n+1/2})_{x_2}), \quad \mathbf{x} \in \omega, \tag{48}$$

$$\begin{aligned} &(\delta p_{\bar{x}_1})_{2,j} = (w_1^{n+1/2})_{2,j}/\tau, \qquad (\delta p_{\bar{x}_1})_{N_1,j} = 0, \quad j = 2,\ 3,\ \ldots,\ N_2 - 1, \\ &(\delta p_{\bar{x}_2})_{i,2} = (w_2^{n+1/2})_{i,2}/\tau, \qquad (\delta p_{\bar{x}_2})_{i,N_2} = 0, \quad i = 2,\ 3,\ \ldots,\ N_1 - 1, \end{aligned} \tag{49}$$

$$\sum_{\mathbf{x} \in \omega^*} \delta p = 0, \tag{50}$$

(iii) evaluation of the velocity and pressure at the next time level,

$$w_\alpha^{n+1} = w_\alpha^{n+1/2} - \tau \cdot \delta p_{\bar{x}_\alpha}, \quad \alpha = 1, 2, \quad \mathbf{x} \in \omega, \tag{51}$$

$$p^{n+1} = p^n + \delta p, \quad \mathbf{x} \in \omega, \tag{52}$$

with the boundary and initial condition

$$\mathbf{w}^n = 0, \quad \mathbf{x} \in \partial\omega, \tag{53}$$

$$\mathbf{w}^0 = \mathbf{v}^0(\mathbf{x}), \quad \mathbf{x} \in \omega. \tag{54}$$

The additional condition (50), which is similar to equation (6) in the differential problem, is introduced only for pressure correction (and pressure) uniqueness.

It should be noted that for the Neumann problem (48)–(50) the compatability constraint must be satisfied. This constraint is an analogue of the compatibility constraint

$$\int_\Omega f \, d\mathbf{x} + \int_{\partial\Omega} \varphi = 0 \tag{55}$$

for the differential problem:

$$\operatorname{div} \operatorname{grad} p = -f, \quad \mathbf{x} \in \Omega, \qquad \frac{\partial p}{\partial \mathbf{n}} = \varphi, \quad \mathbf{x} \in \partial\Omega. \tag{56}$$

It is easy to show that for the problem (48)–(50) the compatability constraint is automatically satisfied. This fact results from the above-mentioned correct formulation of the discrete Poisson equation via algebraic transformations.[26,28,29] The popular way to derive the boundary conditions for the pressure by considering the momentum equations at the boundary does not lead to satisfaction of this constraint by default. Some additional effort must be made in order to satisfy it.[4]

In just the same way we can implement the scheme with the Peaceman–Rachford-type splitting procedure. This scheme includes the Neumann problem for the pressure correction Poisson equation as well.

6. *A PRIORI* ESTIMATE FOR THE SOLUTION OF THE DISCRETE PROBLEM

Now we shall obtain an *a priori* estimate for the solution of the discrete problem (38)–(40) with the Douglas–Rachford-type splitting procedure. We shall essentially use properties (30)–(32) of the operators $V(\mathbf{w})$, P and N.

Let us rewrite equations (38) and (41) in the form

$$(E + \tau A_1)\mathbf{w}^{n+1/2} = (E - \tau A_2)\mathbf{w}^n + \tau \mathbf{f}^n, \tag{57}$$

$$(E + \tau A_2)\mathbf{w}^{n+1} = \mathbf{w}^{n+1/2} + \tau A_2 \mathbf{w}^n, \tag{58}$$

where E is the identity operator.

Let us multiply equation (57) by $(E + \tau A_1)\mathbf{w}^{n+1/2}$, take the scalar product and use the Schwarz inequality. We obtain the inequality

$$\|(E + \tau A_1)\mathbf{w}^{n+1/2}\| \leqslant \|(E - \tau A_2)\mathbf{w}^n\| + \tau \|\mathbf{f}^n\|, \tag{59}$$

which will be used below. Transform the right-hand side of (58) as

$$\begin{aligned}\mathbf{w}^{n+1/2}+\tau A_2\mathbf{w}^n &= \mathbf{w}^{n+1/2}+\tfrac{1}{2}(E+\tau A_2)\mathbf{w}^n-\tfrac{1}{2}(E-\tau A_2)\mathbf{w}^n\\ &= \mathbf{w}^{n+1/2}+\tfrac{1}{2}(E+\tau A_2)\mathbf{w}^n-\tfrac{1}{2}(E+\tau A_1)\mathbf{w}^{n+1/2}+\frac{\tau}{2}\mathbf{f}^n\\ &= \tfrac{1}{2}(E+\tau A_2)\mathbf{w}^n+\tfrac{1}{2}(E-\tau A_1)\mathbf{w}^{n+1/2}+\frac{\tau}{2}\mathbf{f}^n. \end{aligned} \tag{60}$$

When the rearranged right-hand side is substituted, equation (58) becomes

$$(E+\tau A_2)\mathbf{w}^{n+1}=\tfrac{1}{2}(E+\tau A_2)\mathbf{w}^n+\tfrac{1}{2}(E-\tau A_1)\mathbf{w}^{n+1/2}+\frac{\tau}{2}\mathbf{f}^n. \tag{61}$$

Multiply this equation by $(E+\tau A_2)\mathbf{w}^{n+1}$, take the scalar product and use the Schwarz inequality to obtain

$$\|(E+\tau A_2)\mathbf{w}^{n+1}\|\le\tfrac{1}{2}\|(E+\tau A_2)\mathbf{w}^n\|+\tfrac{1}{2}\|(E-\tau A_1)\mathbf{w}^{n+1/2}\|+\frac{\tau}{2}\|\mathbf{f}^n\|. \tag{62}$$

It is well known that for any operator $B\geqslant 0$ the inequality

$$\|(E-B)y\|\leqslant\|(E+B)y\| \tag{63}$$

is valid. Thus, taking into consideration this inequality and inequality (59), we can evaluate the second term on the right-hand side of (62) as

$$\begin{aligned}\|(E-\tau A_1)\mathbf{w}^{n+1/2}\| &\leqslant \|(E+\tau A_1)\mathbf{w}^{n+1/2}\|\\ &\leqslant \|(E-\tau A_2)\mathbf{w}^n\|+\tau\|\mathbf{f}^n\|\\ &\leqslant \|(E+\tau A_2)\mathbf{w}^n\|+\tau\|\mathbf{f}^n\|. \end{aligned} \tag{64}$$

In order to derive the last inequality, in this inequality sequence we have used (63) once more.

Taking account of expression (64) in (62), we can rewrite (62) as

$$\|(E+\tau A_2)\mathbf{w}^{n+1}\|\leqslant\|(E+\tau A_2)\mathbf{w}^n\|+\|\mathbf{f}^n\|. \tag{65}$$

Using the skew-symmetric property of the operator A_2, which is identical with P, and $P\mathbf{w}=\mathrm{grad}_h p$, it is easy to show that

$$\begin{aligned}\|(E+\tau A_2)\mathbf{w}\|^2 &= ((E+\tau A_2)\mathbf{w},\ (E+\tau A_2)\mathbf{w})_2=(\mathbf{w},\mathbf{w})_2+\tau^2(\mathrm{grad}_h p,\ \mathrm{grad}_h p)_2\\ &= \|\mathbf{w}\|^2+\tau^2\|\mathrm{grad}_h p\|^2. \end{aligned} \tag{66}$$

Substitution of (66) into inequality (65) gives

$$\|\mathbf{w}^{n+1}\|_\tau\leqslant\|\mathbf{w}^n\|_\tau+\tau\|\mathbf{f}^n\|, \tag{67}$$

where

$$\|\mathbf{w}\|_\tau=\sqrt{(\|\mathbf{w}\|^2+\tau^2\|\mathrm{grad}_h p\|^2)}.$$

From (67) we can derive the next estimate

$$\|\mathbf{w}^{n+1}\|\leqslant\sqrt{(\|\mathbf{w}^0\|^2+\tau^2\|\mathrm{grad}_h p^0\|^2)}+\Theta\max_{k=0,1,\ldots,n}\|\mathbf{f}^k\|, \tag{68}$$

where $\mathbf{w}^0=\mathbf{v}_0(\mathbf{x})$ and $p^0=p(\mathbf{x},0)$.

This estimate is similar to estimate (12) for the corresponding differential problem. It is unconditional, i.e. it was derived without any restrictions on the parameters τ and h of the discrete problem. Estimate (68) provides boundedness of any solution of the scheme (38)–(40). It also provides unconditional stability in respect of the right-hand side and initial data, but only for the trivial (zero)

solution owing to the fact that the equations are non-linear. We should note that the estimate does not guarantee convergence of the discrete solution.

For the solution of the Peaceman–Rachford-type scheme (36), (37) a similar *a priori* estimate is valid.

7. NUMERICAL RESULTS

The methods developed in the present study have been tested on the lid-driven cavity flow of a viscous incompressible fluid. Time-dependent as well as steady state (as a limit of the time evolution process) solutions have been obtained and extensively compared with the benchmark results of Ghia *et al.*[30] derived on a very fine grid of 257×257 points. Flow regimes with $Re = 100$, 400, 1000 and 3200 have been calculated on the sequence of grids with 21×21, 41×41, 81×81 and 161×161 points. The method (47)–(52) with the Douglas–Rachford-type splitting procedure was used to calculate all solutions depicted below in figures and tables. All predictions have been performed on an IBM PC 486 personal computer.

It should be noted that a non-zero tangential velocity is prescribed at the upper boundary in this problem. It is clear that in the discrete case it is easy to reformulate this problem, so we shall derive the problem with uniform zero boundary conditions (by means of some modifications of the right-hand side). Thus all the above-mentioned properties of the scheme operators are valid for our calculations.

The systems of algebraic equations were solved in this work using the following iterative solvers:[31] a modified incomplete Cholesky conjugate gradient method (ICCG) for the pressure correction Poisson equation and a preconditioned conjugate gradient method (ORTHOMIN(1)) for the asymmetric momentum equations. A very efficient implementation of these popular methods, designed on the basis of recent developments in this field, has been employed in our predictions for the symmetric[32] and asymmetric[33] linear grid equations.

To obtain steady state solutions, the following criterion for the calculation termination has been used:

$$\|\mathbf{w}_\tau\| \leqslant \varepsilon, \tag{69}$$

where $\mathbf{w}_\tau = ((w_1^{n+1} - w_1^n)/\tau,\ (w_2^{n+1} - u_2^n)/\tau)$ and $\varepsilon = 10^{-5}$ everywhere except for Figure 10. The quiescent state was used as the initial condition for time integration.

The aims of the calculations were

(a) to study the dependence of the solution accuracy and the convergence rate on the number of grid points and the time step size τ
(b) to investigate how for a particular problem the solution accuracy depends on the actual choice of the div_h and grad_h approximation among the four possible combinations (26)–(29)
(c) to compare the Douglas–Rachford- and Peaceman–Rachford-type schemes.

Figures 3–6 present the predicted (a) streamlines and (b) isobars (via equidistant isolines) for $Re = 100$, 400, 1000 and 3200 respectively derived on the grid with 161×161 points. Good agreement with the benchmark results of Ghia *et al.*[30] is obtained not only in the global flow patterns for various Re but also in the local flow characteristics.

Table I gives for the steady state solutions the maximum absolute streamfunction value $|\Psi|_{\max}$ and the error norm $\|\mathbf{w} - \mathbf{w}^{\text{bench}}\|_* = \max |\mathbf{w}_{i,j} - \mathbf{w}_{i,j}^{\text{bench}}| \times 100\%$ as a function of the Reynolds number and grid size, where $\mathbf{w}$ is the velocity from our predictions, $\mathbf{w}^{\text{bench}}$ is the benchmark numerical solution of Ghia *et al.*[30] and the error norm $\|\cdot\|_*$ is calculated over the points of the horizontal and vertical centrelines using the corresponding velocity component (the horizontal velocity at the vertical centreline and vice versa; see Figure 7). Only the best results (among the four possible combinations

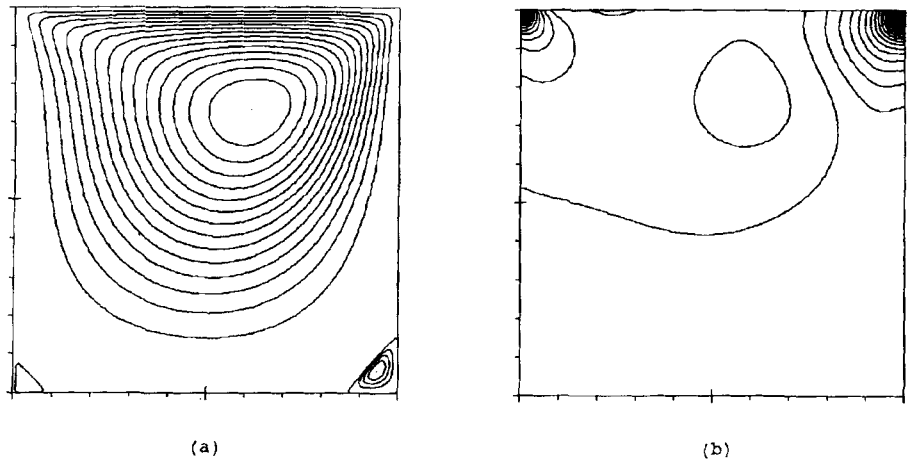

Figure 3. (a) Streamlines and (b) isobars for $Re = 100$

(26)–(29)) are presented in this table. Formally the schemes under consideration have first-order accuracy in space. The results presented in Table I show that the order of accuracy of the schemes is indeed the first (asymptotically). In spite of only first-order accuracy, the scheme provides reasonable agreement with the benchmark solution (at least at $Re \leqslant 1000$) on the fine grid.

The results in Figure 7 and Table II demonstrate the dependence of the solution accuracy on the actual choice of the div_h and grad_h approximation among the four possible cases of consistent first-order approximations. Figure 7 shows the predicted velocity profiles—the four full curves correspond to the four different approximations (26)–(29)—along the vertical and horizontal cavity centrelines for $Re = 400$ on the grids with (a) 21×21 and (b) 81×81 points. The benchmark solution of Ghia *et al.*[30] is also depicted in this figure via symbols for comparison. It should be noted again that all these approximation combinations (26)–(29) are equivalent from the theoretical viewpoint but yield somewhat different prediction accuracies. The solution accuracy depends essentially (on a coarse grid) on the orientation of the moving cavity wall with respect to the direction of differencing in the above-mentioned couples of discrete operators. Moreover, it is not possible to decide *a priori* which couple is

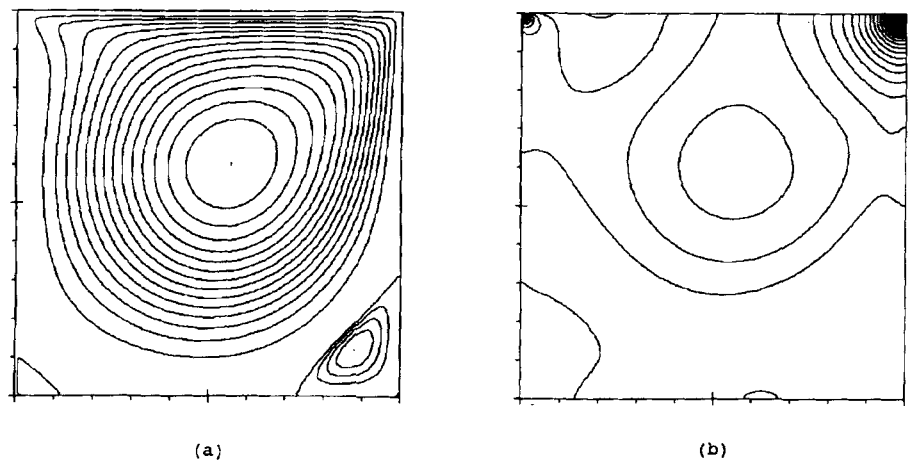

Figure 4. (a) Streamlines and (b) isobars for $Re = 400$

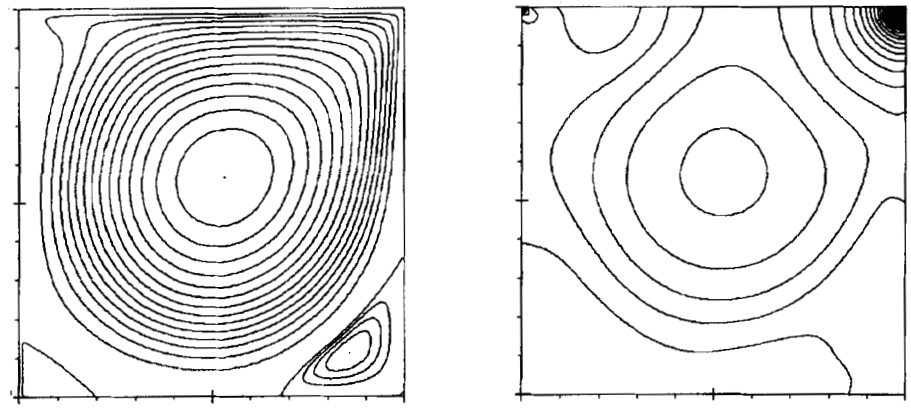

Figure 5. (a) Streamlines and (b) isobars for $Re = 1000$

preferable for a particular flow, but evidently (compare (a) and (b) in Figure 7) the distinction between the four possible approximations decreases drastically with refinement of the computational grid. In Table II the values of $|\Psi|_{max}$ and $\|\mathbf{w} - \mathbf{w}^{bench}\|_*$ are presented for the worst and best cases at $Re = 400$ on various grids. It is clear that for this particular problem the predictions in the best case are twice as accurate as those in the worst case.

The effects of the spatial grid size and the time step size τ on the time-dependent solution accuracy have also been studied. The history of $|\Psi|_{max}$ is shown in Figure 8 for various time steps τ at $Re = 1000$ on the 81×81 grid. The results indicate that the time-dependent solution is sufficiently accurate at $\tau \leqslant 0{\cdot}25$, but a much larger time step can be used if only the steady state solution is studied. For $\tau > 3$ the solution becomes oscillating and the convergence criterion (69) is not reached. Figure 9 demonstrates the effect of the spatial grid size on the time evolution of $|\Psi|_{max}$ at the same Reynods number and fixed $\tau = 0{\cdot}1$. The time step τ is chosen small enough in order to reduce the effect of the truncation error due to time discretization.

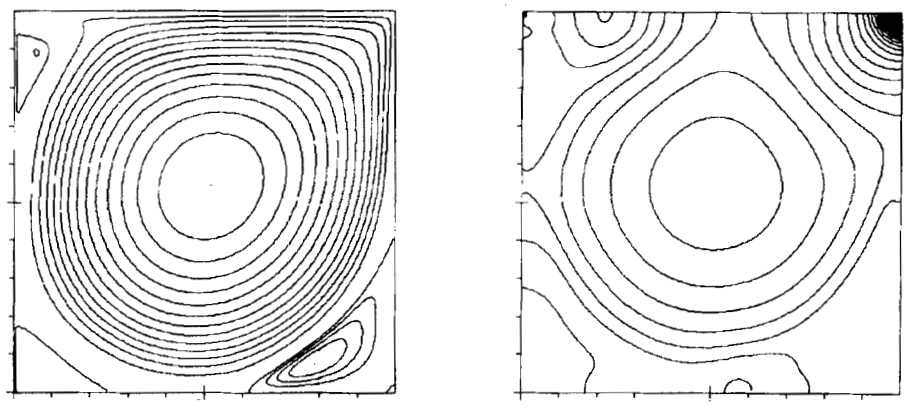

Figure 6. (a) Streamlines and (b) isobars for $Re = 3200$

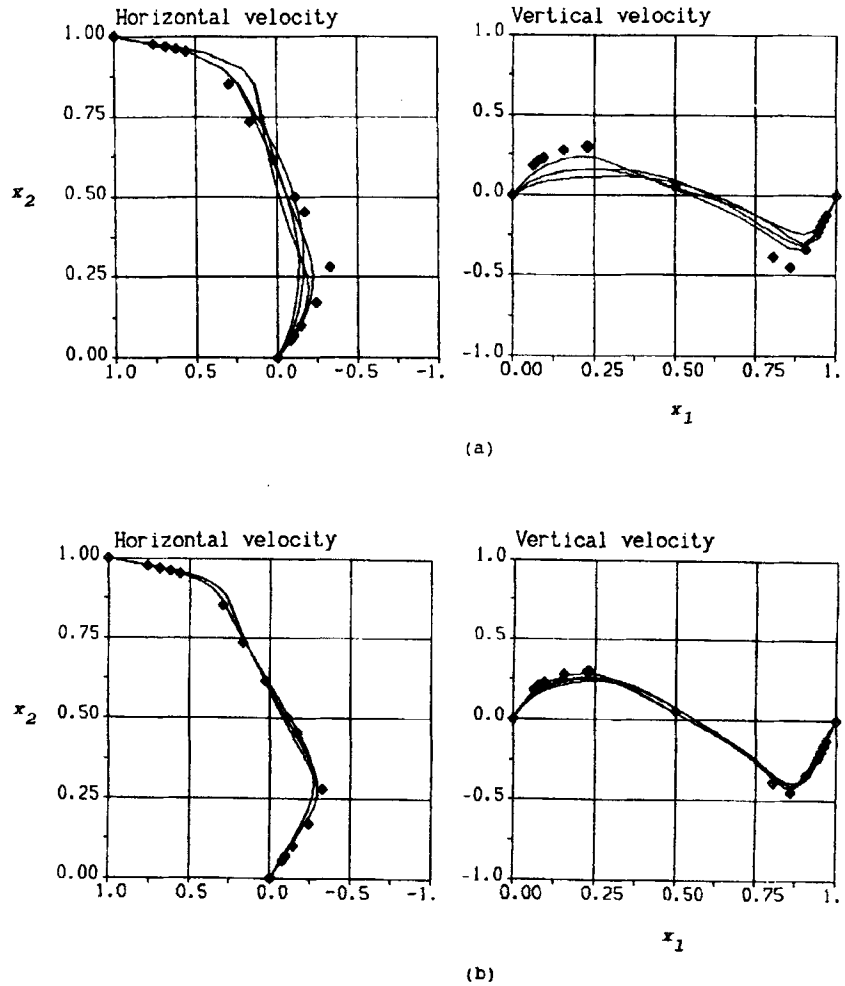

Figure 7. Velocity profiles along centrelines for $Re = 400$ on (a) 21×21 and (b) 81×81 grid:s full curves, present work for various approximations; symbols, Ghia *et al.*'s benchmark solution[30]

The dependence of the time step number required for the achievement of the steady state solution (with the same convergence criterion (69) but $\varepsilon = 10^{-4}$) on the time step size τ is presented in Figure 10 for $Re = 1000$ and various spatial grids. It is clear, that (i) the number of time steps increases very weakly with increasing spatial grid size and (ii) there is an optimal time step value (in the vicinity of $\tau = 1$ for this particular problem and flow regime) that provides the minimum number of integration steps. It should be noted that the scheme provides stable calculations at a much larger time step than the optimal one and the limit of stability depends very weakly on the number of grid points. In some papers the normalized time step $\alpha = \tau/h^2 Re$, which is associated with the diffusion limit of the explicit scheme, was used in order to characterize the stability restriction on the time step τ. For the present method on the grid with 161×161 points and $Re = 1000$, for example, the maximum value allowing stable computations was $\alpha = 64$, which is much higher in comparison with traditional computational procedures. Moreover, the parameter α is not suitable for characterizing the stability restriction owing to the fact that in our scheme τ is not linearly proportional to h^2.

It should be noted again that we solve the time-dependent incompressible Navier–Stokes equations and the analysis provided here indicates that the methods developed are absolutely stable in a linear

Table I. Dependence of solution accuracy on spatial grid size for various Reynolds numbers

Re	$\|\Psi\|_{max}$ (Ghia *et al.*[30])	$N_1 \times N_2$	$\|\Psi\|_{max}$	$\|\mathbf{w} - \mathbf{w}^{bench}\|_*$ (%)
100	0·1034	21 × 21	0·085	4·49
		41 × 41	0·095	2·41
		81 × 81	0·099	1·55
		161 × 161	0·1014	1·00
400	0·1139	21 × 21	0·081	12·29
		41 × 41	0·095	6·44
		81 × 81	0·104	3·09
		161 × 161	0·109	2·87
1000	0·1179	21 × 21	0·068	19·7
		41 × 41	0·085	12·06
		81 × 81	0·100	8·28
		161 × 161	0·109	4·09
3200	0·1204	21 × 21	0·046	25·89
		41 × 41	0·056	25·02
		81 × 81	0·082	19·75
		161 × 161	0·099	10·14

Table II. Dependence of solution accuracy on grid size and stencil: worst/best values for $Re = 400$

$N_1 = N_2$	$\|\Psi\|_{max}$	$\|\mathbf{w} - \mathbf{w}^{bench}\|_*$ (%)
21	0·058/0·081	22·76/12·29
41	0·082/0·095	12·8/6·44
81	0·098/0·104	6·35/3·09
257*	0·1139	

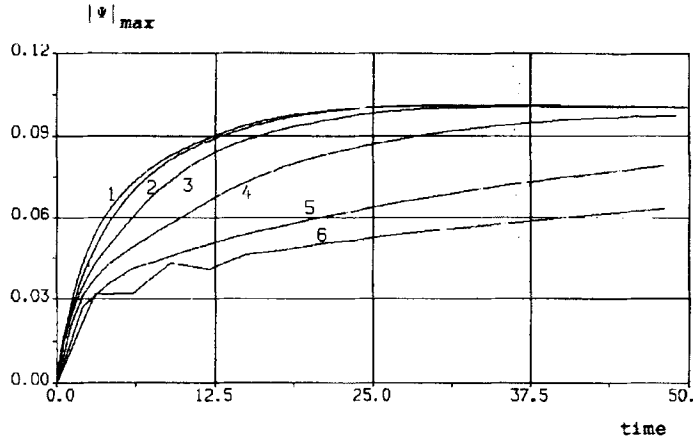

Figure 8. History of $|\Psi|_{max}$ for $Re = 1000$ at various time steps: 1, $\tau = 0{\cdot}25$; 2, $\tau = 0{\cdot}1$; 3, $\tau = 0{\cdot}5$; 4, $\tau = 1$; 5, $\tau = 2$; 6, $\tau = 3$

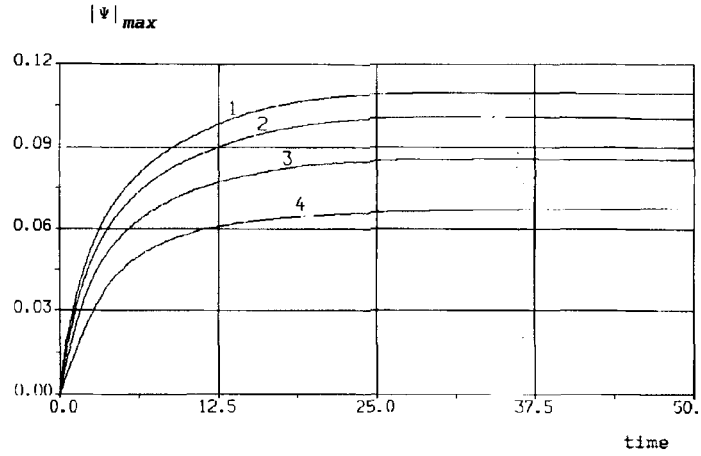

Figure 9. Dependence of $|\Psi|_{max}$ on grid size for $Re = 1000$: 1, 161 × 161; 2, 81 × 81; 3, 41 × 41; 4, 21 × 21

sense. Returning to the above-mentioned figures, it is easy to see that these schemes allow us to use a much larger time step for integration in time in comparison with traditional computational techniques for unsteady convection–diffusion problems (see Figure 8) and that the stability limit for our schemes does not depend practically on the grid size (see Figure 10), i.e. this limit exists only as a result of the non-linearity of the Navier–Stokes equations, which is not resolved in our linearized difference schemes. Thus, to study transient flow problems, we can choose a time step only from considerations of the temporal accuracy which is necessary to describe a non-linear phenomenon in detail.

To validate these new schemes on transient problems, the unsteady cavity problem (i.e. the flow inside a cavity with an impulsively started lid) has been studied numerically and the results compared

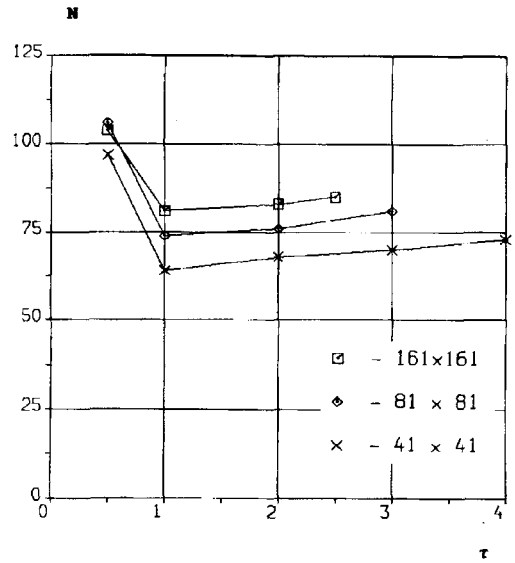

Figure 10. Number of integration steps N for achievement of steady state solution versus time step size τ for $Re = 1000$ on various grids

Table III. Increase in time step size τ during integration in time for unsteady cavity problem

t	$0 \leqslant t \leqslant 1$	$1 < t \leqslant 2$	$2 < t \leqslant 4$	$t > 4$
τ	0·02	0·04	0·05	0·1

with time-accurate solutions obtained by Son and Goodrich.[34] The results in Reference 34 are very accurate as they were obtained using a scheme of second-order accuracy in space and time with fully implicit implementation of non-linearity and incompressibility constraints at every time level (via some iterative procedure). Moreover, to provide high resolution of the evolving boundary layer, it was suggested in that work to use a varying time step with stepwise increases during time integration. Our predictions of this problem on the grid with 161×161 points for $Re = 400$ and 800 are presented in Figures 11 and 12 respectively. In these figures the development of the flow is shown via the flow patterns at time instants $t = 0{\cdot}1$, 1, 2, 4 and 8. Along with the equidistant streamlines, the streamfunction extrema are reported as well. The time variation of the time step size employed in our calculations is presented in Table III. It was obtained in a similar way as in Reference 34 but for our grid size and $Re = 800$. Comparison of our solutions for $Re = 400$ depicted in Figure 11 with the accurate results (see Figure 5 of Reference 34) indicates good temporal accuracy of our predictions. Good agreement is obtained for the time evolution of primary and secondary vortices. Secondary vortices near the lower wall corners appear as early as $t = 2$ and grow in size (see values of $\psi_{\max}$ in Figure 11). A more complicated history of the flow evolution is evident in Figure 12 for $Re = 800$. All these results demonstrate the efficiency of the proposed method in application to transient flow problems.

All the above-mentioned (both theoretical and practical) results have been obtained for Dirichlet boundary conditions, i.e. for a somewhat restricted class of fluid flow problems. To examine the robustness of the present methods and the possibility of modelling channel flows with 'open' boundary conditions, the flow over a backward-facing step[35–38] has been predicted and compared for a wide range of Reynolds numbers without any theoretical proofs.

This flow has been studied numerically using a uniform 161×41 grid and the Douglas–Rachford-type splitting procedure (38), (39) in the problem formulation by Kim and Moin.[36] A parabolic velocity profile is prescribed at the inlet, whereas Neumann-type conditions—zero normal derivatives for both velocity components—are imposed at the outlet of the computational domain. It is well known[39] that these conditions are the simplest but, as a rule, the worst 'open' boundary conditions. Nevertheless, steady state numerical solutions have been obtained in our predictions for flows with $Re = 200$, 400, 600 and even such a 'critical' value as $Re = 800$ (critical not in the sense of some kind of flow transition but in the sense of involving a considerable and long-term scientific discussion[40]). Figure 13 illustrates our steady state numerical results for $Re = 800$ via (a) equidistant streamlines and (b) isobars (see Reference 37 for a comparison). In all four cases (including $Re = 800$), reasonable qualitative agreement with benchmark solutions[36–38] has been obtained. Some quantitative discrepancies in the sizes of recirculating zones at the upper and lower walls (especially for $Re = 800$) may be explained by the following considerations: first, we used a shorter channel length (16 instead of 30 as in Reference 37) along with less soft 'open' boundary conditions; secondly, our scheme provides only first-order-accurate results. Nevertheless, these results indicate that our approach is robust and applicable to modelling channel flows too.

It is necessary to emphasize two main special features that have emerged in this study. First, the linearized schemes derived here have a very weak time step restriction (due to non-linearity). The time

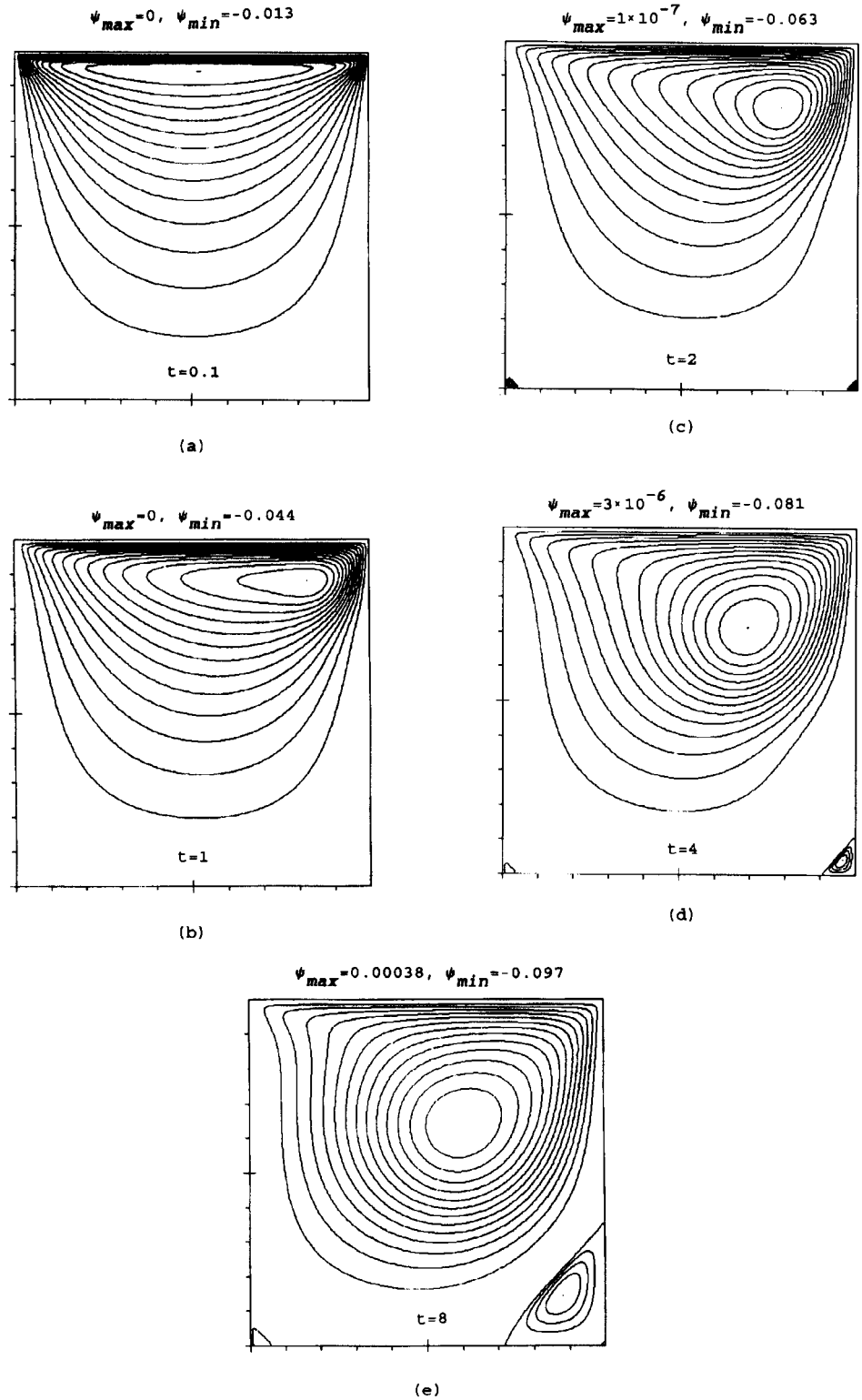

Figure 11. Time evolution of unsteady cavity flow for $Re = 400$: (a) $t = 0{\cdot}1$; (b) $t = 1$; (c) $t = 2$; (d) $t = 4$; (e) $t = 8$

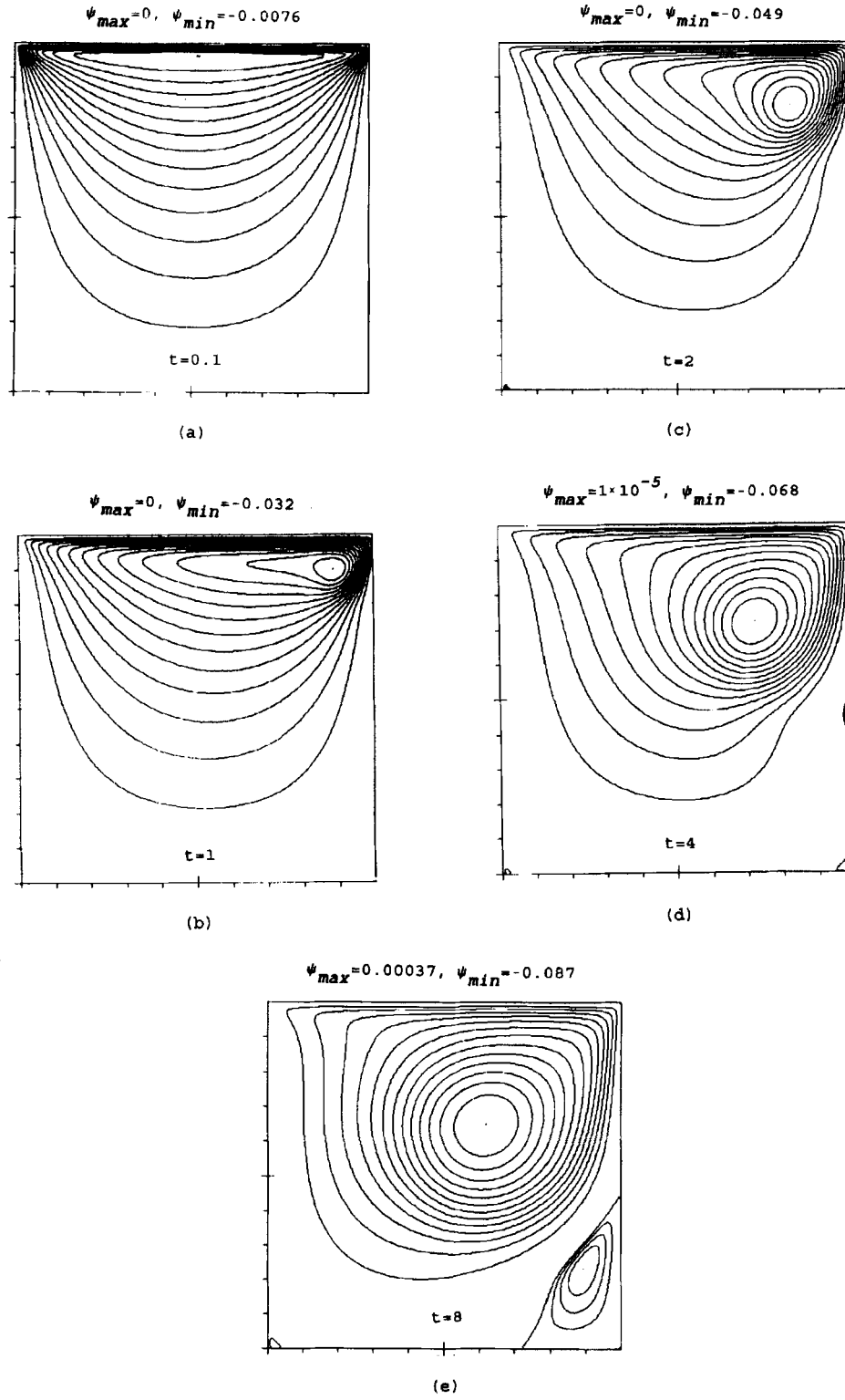

Figure 12. Time evolution of unsteady cavity flow for $Re = 800$: (a) $t = 0{\cdot}1$; (b) $t = 1$; (c) $t = 2$; (d) $t = 4$; (e) $t = 8$

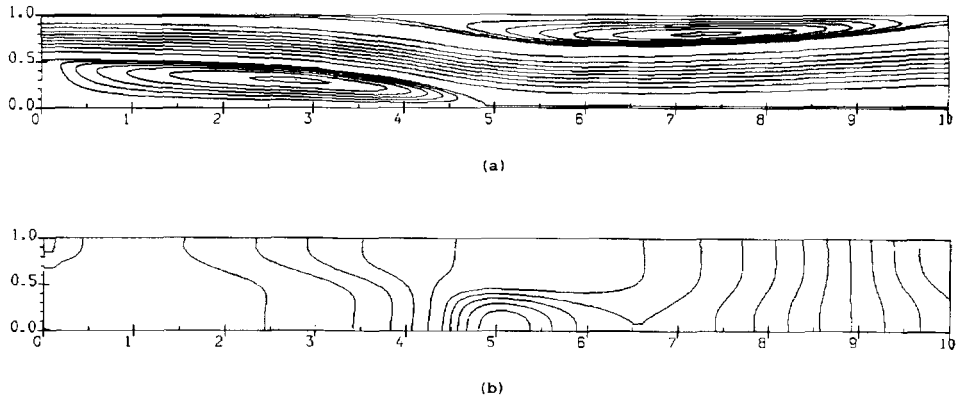

Figure 13. (a) Streamlines and (b) isobars for flow over a backward-facing step, $Re = 800$

step value is chosen moderate enough only in order to obtain sufficiently time-accurate solutions when transient problems are considered.

Secondly, it was found that the maximum time step value τ_{max} at which convergence is achieved for the Peaceman–Rachford-type method is about 25 times smaller than τ_{max} for the Douglas– Rachford-type scheme. Since both methods are accurate enough at time step values which are needed for convergence of the Peaceman–Rachford-type method, the Douglas–Rachford-type splitting method is certainly preferred over the Peaceman–Rachford technique.

8. CONCLUSIONS

1. Absolutely stable (in a linear sense) methods for solving the time-dependent incompressible Navier–Stokes equations using primitive variables and non-staggered grids are developed and verified in the present work. The operators of the linearized difference schemes are consistent with one another and inherit the fundamental properties of the corresponding differential operators of the initial differential equations. These schemes inherit *a priori* estimates for their solutions as well.
2. Special second-order approximations based on central differences are used for convective terms. No upwinding or artificial viscosity is employed to monotonize the schemes.
3. To avoid checker-board effects on the non-staggered grid, first-order opposite (forward and backward) differences are utilized to approximate the divergence and gradient operators. Practical calculations indicate that such approximations actually provide first-order accuracy of the numerical solution. The use of second-order approximations for these operators will be presented in the next part of this work.
4. Of the two considered operator-splitting procedures adapted for time discretization, the Douglas–Rachford-type scheme is certainly preferred over the Peaceman–Rachford-type one from the viewpoint of stability.
5. The issue of 'open' (outflow, non-Dirichlet) boundary conditions remains open (in a theoretical sense) in the present study; it is to be investigated (in the framework of the developed approach) in the immediate future. However, practical predictions of a backward-facing step flow with the simplest 'open' conditions (i.e. of the Neumann type for both velocity components at the outlet) indicate that the methods developed here remain robust and efficient for channel flow predictions as well.

ACKNOWLEDGEMENTS

The authors would like to thank Dr. Vladimir V. Chudanov and Dr. Mikhail M. Makarov for helpful suggestions and comments. This work was supported by the Russian Fundamental Investigation Foundation under grant 94-01-01448.

REFERENCES

1. S. V. Patankar, *Numerical Heat Transfer and Fluid Flow*, Hemisphere, Washington, DC, 1980.
2. F. H. Harlow and J. E. Welch, 'Numerical calculation of time-dependent viscous incompressible flow of fluid with free surface', *Phys. Fluids*, **8**, 2182–2189 (1965).
3. M. Reggio and R. Camarero, 'Numerical solution procedure for viscous incompressible flows', *Numer. Heat Transfer*, **10**, 131–146 (1986).
4. S. Abdallah, 'Numerical solutions for the incompressible Navier–Stokes equations in primitive variables using a non-staggered grid, II', *J. Comput. Phys.*, **70**, 193–202 (1987).
5. G. E. Schneider and M. J. Raw, 'Control volume finite-element method for heat transfer and fluid flow using colocated variables. 1. Computational procedure', *Numer. Heat Transfer*, **11**, 363–390 (1987).
6. M. Peric, R. Kessler and G. Scheuerer, 'Comparison of finite-volume numerical methods with staggered and colocated grids', *Comput. Fluids*, **16**, 389–403 (1988).
7. T. M. Shih, C. H. Tan and B. C. Hwang, 'Effects of grid staggering on numerical schemes', *Int. j. numer. methods fluids*, **9**, 193– 212 (1989).
8. M. L. Mansour and A. Hamed, 'Implicit solution of the incompressible Navier–Stokes equations on a non-staggered grid', *J. Comput. Phys.*, **86**, 147–167 (1990).
9. M. H. Kobayashi and J. C. F. Pereira, 'Numerical comparison of momentum interpolation methods and pressure–velocity algorithms using non-staggered grids', *Commun. Appl. Numer. Methods*, **7**, 173–186 (1991).
10. P. Coelho, J. C. F. Pereira and M. G. Carvalho, 'Calculation of laminar recirculating flows using a local non-staggered grid refinement system', *Int. j. numer. methods fluids*, **12**, 535–557 (1991).
11. S. W. Armfield, 'Finite difference solutions of the Navier–Stokes equations on staggered and non-staggered grids', *Comput. Fluids*, **20**, 1–17 (1991).
12. F. Sotiropoulos and S. Abdallah, 'A primitive variable method for the solution of three-dimensional incompressible viscous flows', *J. Comput. Phys.*, **103**, 336–349 (1992).
13. A. S. Dvinsky and J. K. Dukowicz, 'Null-space-free methods for the incompressible Navier–Stokes equations on non-staggered curvilinear grids', *Comput. Fluids*, **22**, 685–696 (1993).
14. O. A. Ladysenskaya, *The Mathematical Theory of Viscous Incompressible Flows*, Gordon and Breach, New York, 1969.
15. R. Temam, *Navier–Stokes Equations, Theory and Numerical Analysis*, North-Holland, Amsterdam, 1984.
16. N. N. Yanenko, *The Method of Fractional Steps*, Springer, New York, 1971.
17. G. I. Marchuk, *Methods of Numerical Mathematics*, Springer, Berlin, 1982.
18. A. A. Samarskii, *Theory of Difference Schemes*, Nauka, Moscow, 1989 (in Russian).
19. O. Pironneau, 'On the transport-diffusion algorithm and its applications to the Navier–Stokes equations', *Numer. Math.*, **38**, 309–332 (1982).
20. M. O. Bristeau, R. Glowinski and J. Periaux, 'Numerical methods for the Navier–Stokes equations. Applications to the simulation of compressible and incompressible viscous flows', *Comput. Phys. Rep.*, **6**, 73–187 (1987).
21. R. Glowinski and P. Le Tallec, *Augmented Lagrangian Methods and Operator-Splitting Methods in Nonlinear Mechanics*, SIAM, Philadelphia, PA, 1989.
22. Y. Maday, A. T. Patera and E. M. Ronquist, 'An operator–integration-factor splitting method for time-dependent problems: application to incompressible fluid flow', *J. Sci. Comput.*, **5**, 263–292 (1990).
23. R. Natarajan, 'A numerical method for incompressible viscous flow simulation', *J. Comput. Phys.*, **100**, 384–395 (1992).
24. D. W. Peaceman and H. H. Rachford, Jr., 'The numerical solution of parabolic and elliptic differential equations', *SIAM J.*, **3**, 28–41 (1955).
25. J. Douglas and H. H. Rachford, 'On the numerical solution of heat conduction problems in two and three space variables', *Trans. Am. Math. Soc.*, **82**, 421–439 (1956).
26. P. M. Gresho, 'Incompressible fluid dynamics: some fundamental formulation issues', *Ann. Rev. Fluid Mech.*, **23**, 413–453 (1991).
27. A. A. Samarskii and E. S. Nikolaev, *Numerical Methods for Grid Equations*, Vols 1 and 2, Birkhauser, Basle, 1989.
28. P. M. Gresho and R. L. Sani, 'On pressure boundary conditions for the incompressible Navier–Stokes equations', *Int. j. numer. methods fluids*, **7**, 1111–1145 (1987).
29. A. E. P. Veldman, ' "Missing" boundary conditions? Discretize first, substitute next, and combine later', *SIAM J. Sci. Stat. Comput.*, **11**, 82–91 (1990).
30. U. Ghia, K. N. Ghia and C. T. Shin, 'High-*Re* solutions for incompressible flow using the Navier–Stokes equations and a multigrid method', *J. Comput. Phys.*, **48**, 387–411 (1982).
31. L. A. Hageman and D. M. Young, *Applied Iterative Methods*, Academic, New York, 1981.
32. A. B. Kutcherov and M. M. Makarov, 'An approximate factorization method for solving finite-difference elliptic problems with mixed boundary conditions', in *Numerical Methods in Mathematical Physics*, Moscow State University, Moscow, 1984, pp. 54–65 (in Russian).

33. O. P. Iliev, M. M. Makarov and P. S. Vassilevski, 'Performance of certain iterative methods in solving implicit difference schemes for 2-D Navier–Stokes equations', *Int j. numer. methods eng.*, **33**, 1465–1479 (1992).
34. W. Y. Son and J. W. Goodrich, 'Unsteady solution of incompressible Navier–Stokes equations', *J. Comput. Phys.*, **79**, 113–134 (1988).
35. B. F. Armaly, F. Durst, J. C. F. Pereira and B. Schonung, 'Experimental and theoretical investigation of backward-facing step flow', *J. Fluid Mech.*, **127**, 473–496 (1983).
36. J. Kim and P. Moin, 'Application of a fractional-step method to incompressible Navier–Stokes equations', *J. Comput. Phys.*, **59**, 308–323 (1985).
37. D. K. Gartling, 'A test problem for outflow boundary conditions—flow over a backward-facing step', *Int. j. numer. methods fluids*, **11**, 953–967 (1990).
38. H. Le and P. Moin, 'An improvement of fractional step methods for the incompressible Navier–Stokes equations', *J. Comput. Phys.*, **92**, 369–379 (1991).
39. R. L. Sani and P. M. Gresho, 'Résumé and remarks on the Open Boundary Condition Minisymposium', *Int. j. numer. methods fluids*, **18**, 983–1008 (1994).
40. P. M. Gresho, D. K. Gartling, J. R. Torczynski, K. A. Cliffe, K. H. Winters, T. J. Garratt, A. Spence and J. W. Goodrich, 'Is the steady viscous incompressible two-dimensional flow over a backward-facing step at $Re = 800$ stable?', *Int. j. numer. methods fluids*, **17**, 501–541 (1993).